Journal Pre-proof

Time-temperature indicator based on the variation of the optical response of photonic crystals upon polymer infiltration

Luisa G. Cencha, Guadalupe F. García, Nicolás Budini, Raúl Urteaga, Claudio L.A. Berli

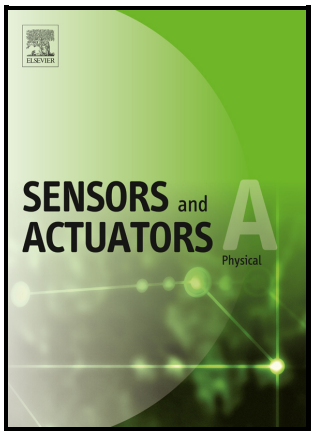

PII: S0924-4247(22)00209-6

DOI: https://doi.org/10.1016/j.sna.2022.113571

Reference: SNA113571

To appear in: *Sensors and Actuators: A. Physical*

Received date: 1 October 2021
Revised date: 23 March 2022
Accepted date: 12 April 2022

Please cite this article as: Luisa G. Cencha, Guadalupe F. García, Nicolás Budini, Raúl Urteaga and Claudio L.A. Berli, Time-temperature indicator based on the variation of the optical response of photonic crystals upon polymer infiltration, *Sensors and Actuators: A. Physical,* (2021) doi:https://doi.org/10.1016/j.sna.2022.113571

Time-temperature indicator based on the variation of the optical response of photonic crystals upon polymer infiltration

Luisa G. Cencha[1], Guadalupe F. García[2], Nicolás Budini[2], Raúl Urteaga[2], Claudio L. A. Berli[1,*]

[1]INTEC (Universidad Nacional del Litoral - CONICET), Predio CCT-CONICET Santa Fe, RN 168, 3000, Santa Fe, Argentina.

[2]IFIS-Litoral (Universidad Nacional del Litoral - CONICET), Güemes 3450, 3000, Santa Fe, Argentina.

*Corresponding author (Claudio L. A. Berli). E-mail address: cberli@santafe-conicet.gov.ar
Tel.: +54 3424511595; Fax: +54 3424511079.

Keywords:
Time-temperature sensors,
Distributed Bragg reflector,
Polymer infiltration,
Food quality,
Perishable products

Time-temperature indicator based on the variation of the optical response of photonic crystals upon polymer infiltration

Luisa G. Cencha[1,1], Guadalupe F. García[1], Nicolás Budini[1,1], Raúl Urteaga[1,1], Claudio L. A. Berli[1]

Abstract

Time-temperature indicators are used for sensing the thermal history of perishable products, like food and pharmaceutical goods. Their working principle is based on a temperature response that mimics the temperature dependence of the deterioration kinetics of a given product. For successful implementation, time-temperature indicators must be of minimum size, cost-effective, change-irreversible, and easy to read. This work presents a time-temperature sensor based on capillary imbibition of thermoplastic polymers into a mesoporous photonic crystal, which was tuned to reflect well-defined wavelengths of visible light. The photonic crystal was made by electrochemical etching of silicon, where a periodic structure was formed with microscale layers of alternating nanoscale porosity. Polymer infiltration induces an irreversible change of the effective refractive index of the crystal, leading to a progressive shift of the reflected light that can be seen by the naked eye. Importantly, the employed thermoplastic polymer (poly(ethylene vinyl-acetate)) presents a temperature-dependent viscosity that is well represented by the Arrhenius law, which is normally used to characterize the temperature-dependence of quality indexes. Therefore, each reflected color is associated to the time-temperature history of the system, representing the deterioration level of a monitored product.

Keywords: Time-temperature sensors, Distributed Bragg reflector, Polymer infiltration, Food quality, Perishable products

1. Introduction

Time-temperature indicators (TTIs) are devices designed for sensing the thermal history undergone by packaged perishable products and hence to predict its residual shelf-life [1]. These devices are increasingly demanded for monitoring the quality of food and pharmaceutical products during transportation and distribution, as demonstrated by the broad list of existing prototypes [2, 3]. Furthermore, nowadays TTIs enter the so-called smart packaging concept, where sensing, actuating, and communicating are key functions for handling the information on a products' quality in real time [4–6].

From the point of view of the technology target profile, TTIs must be of minimum size to be accommodated in packaging, cost-effective for mass production, change-irreversible

*Corresponding author. Tel.: +54 3424511595; fax: +54 3424511079.
Email address: cberli@santafe-conicet.gov.ar (Claudio L. A. Berli)

for the safety of the output signal, and easy to read for users. From the point of view of the working principle, TTIs should react to temperature changes and produce easy readouts; furthermore, the changes should follow as close as possible the time-dependent deterioration of a given quality index (QI) of the product. Following these requirements, the developed TTIs regularly mimic an Arrhenius-like temperature variation and produce an optical output signal. Sharing these common features, TTIs are usually characterized according to the sensing mechanism: chemical [7–9], microbiological [10, 11], enzymatic [12–14], or physicochemical [15–17]. These are a few arbitrary examples of reported TTIs; detailed lists of devices can be found in the comprehensive reviews mentioned above [2, 3].

Here we report the development of a TTI based on the variation of the optical response of a photonic crystal upon polymer infiltration. The photonic crystal is made by electrochemical etching of silicon [18], where a periodic structure is formed with microscale layers of alternating nanoscale porosity [19]. The mesoporous matrix thus constitutes a distributed Bragg reflector (DBR), which is tuned to reflect visible light of a well-defined wavelength. The inset of Figure 1 shows an electronic microscopy image of a porous silicon Bragg, where the alternating layers are formed by pores of different mean radius, and consequently different porosity and refractive index. The optical variation is produced by allowing the capillary imbibition of a thermoplastic polymer into the crystal, which induces an irreversible change of the reflected light wavelength, i.e. a color change that can be readily seen by the naked eye. A key aspect is that the employed thermoplastic polymer (poly(ethylene vinyl-acetate), pEVA) presents a temperature-dependent viscosity that is well represented by the Arrhenius law [20]. Therefore, the filling degree of the DBR, and hence the reflected color, depends on the undergone time-temperature history, which represents the deterioration level of the monitored product, as well as the remaining shelf-life.

It is worth mentioning that the main problems limiting the use of commercial TTIs are associated to safety, inaccuracy, and high costs [2]. Some available TTIs include toxic compounds that may migrate into perishable products like food, threatening users' safety. On the other hand, the accuracy of commercial TTIs is limited because the response of the sensors depends on several factors other than temperature (pH, light, humidity). For example, for enzymatic/biological TTIs, the presence of antimicrobials/microbes in the ambient directly affects the expected temperature response. For polymerization-based TTIs, the polymerization reaction can be accelerated by the sunlight or direct bright light, which may cause inaccurate readouts (a detailed revision of these issues can be found in [2]).

In the TTI proposed in this work, both safety and inaccuracy drawbacks were minimized. The basic constituents of our sensor (pEVA and porous Si) are non-toxic [21] and, in particular, EVA copolymers were approved by the FDA for use in contact with food surfaces [22]. Besides, since the complex viscosity of pEVA is strongly dependent on temperature [20] and practically insensitive to other ambient factors like humidity, light, pH, or biological activity, the specificity our sensing mechanism improves over that of other reported TTIs. Concerning the third mentioned drawback (relatively high cost as a limiting factor for applications), it should be noted the TTI we are presenting here is rather simple, without mobile parts nor external energy sources, which makes the device quite affordable. Moreover, the main cost comes from the crystalline, highly-doped mΩ·cm Si wafers employed to obtain porous silicon. Nevertheless, this material could

be replaced by low-cost silicon substrates (standard resistivity, 10 Ω·cm [23]), without compromising the TTI sensitivity.

Before detailed descriptions in next sections, here we need to briefly compare our system against previously reported devices with (a priori) similar mechanisms. Indeed, there are several TTIs based on capillary imbibition, however they employ distance-based measurements, which are marked by (i) the change of transmittance of the liquid filled porous substrate [16, 24, 25], (ii) the alteration of the legibility of a printed code after the substrate deformation by the infiltrated liquid [26], or (iii) the change of color produced by the temperature-dependent diffusion of colored substances into the porous substrate [27]. Also based on polymer infiltration, highly sensitive temperature sensors have been recently reported [28–31]; nevertheless, these works do not include TTIs to estimate the residual shelf-life of perishable products, which is the motivation of the present work. On the other hand, a reported TTI that claims the use of temperature-responsive photonic crystals actually employs a hydrogel that deforms, and eventually degrades, when reaching a threshold temperature [32]. Another development that claims a photonic crystal makes use of particulate materials, whose lattice spacing varies with temperature and gets frozen when put in contact with a moving hardener like ethanol, which is stored in a pouch and acts as a timer [33]. As an improved alternative, the system proposed here employs capillary imbibition of polymers into a rigid photonic crystal to produce a broad range of intense and well-defined colors, which can be chosen from the design of the periodic mesoporous matrix. Besides, the device is a very thin sheet, which is easy to pack, does not involve mobile parts nor require energy supply, and provides a simple and intuitive readout.

2. Theory

2.1. Kinetics of quality indexes

The deterioration of food quality and perishable products is associated to chemical, biochemical, bacteriological and/or physical changes. The reaction kinetics may differ in each case, for example zero-order for Maillard reaction or first-order for bacteriological growth [34]; nevertheless, the temperature-dependence of the rate constant k is invariably modeled with the Arrhenius law [3, 34]

$$k(T) = k_0 \exp\left(-\frac{E}{RT}\right), \tag{1}$$

where k_0 is the so-called pre-exponential factor, E the activation energy, R is the gas constant, and T is the absolute temperature. The activation energy gauges the relevance of temperature changes on the deterioration rate of the product quality, thus its magnitude must be closely copied by the designed TTI, in the temperature range of interest. More precisely, the loss of shelf-life is normally evaluated by monitoring a characteristic QI (flavor, color, toxin levels, or microbial load). The correlation of the TTI response to the QI is given by the cumulative time during which the product has been exposed to a time-dependent temperature $T(t)$ [35]. For this purpose, here we use the following integer function

$$I = \frac{1}{k(T_{\text{ref}})} \int_0^t k(T)\mathrm{d}t, \tag{2}$$

where T_{ref} is the reference temperature, normally chosen as the recommended storage temperature. Furthermore, the shelf-life (SL), the time a product may be stored without becoming unsuitable, is tabulated for given reference temperatures [36]. Therefore, the residual shelf-life ($RSL = SL - I$), which is an essential requirement for both consumers and manufacturers, can be quantified as

$$RSL = SL - \exp\left(\frac{E_{QI}}{RT_{\mathrm{ref}}}\right)\int_0^t \exp\left(-\frac{E_{QI}}{RT}\right)\mathrm{d}t, \tag{3}$$

where E_{QI} is introduced as the activation energy for a defined quality index. In what follows we discuss the sensing mechanism of the proposed TTI and, importantly, how to tune its activation energy (E_{TTI}) to match E_{QI}.

2.2. Capillary imbibition in the porous matrix

The velocity of fluid imbibition in porous media follows the classical Lucas-Washburn (LW) dynamics, $\mathrm{d}z/\mathrm{d}t \sim 1/z$, where z is the position of the fluid front at time t [37, 38]. This simple result involves open tubes, absence of evaporation, negligible gravity effects, and a steady balance between Laplace driving force and viscous resistance, i.e., inertia-free dynamics. The proportionality constant between $\mathrm{d}z/\mathrm{d}t$ and $1/z$ depends on both the fluid and porous matrix characteristics; therefore, a model is required for further descriptions. The simplest physical representation is the capillary bundle model [38], which considers an arrangement of non-interconnected, straight capillaries, aligned in the flow direction, for which the LW dynamics results in

$$\frac{\mathrm{d}z}{\mathrm{d}t} = \frac{\gamma(\cos\theta)r_{\mathrm{eff}}}{4\mu}\frac{1}{z}, \tag{4}$$

where μ is the fluid viscosity, γ is the surface tension, θ is the meniscus contact angle, and r_{eff} is the effective radius. Then the imbibition dynamics results $z^2 = D_c t$ where the proportionality constant $D_c = \gamma(\cos\theta)r_{\mathrm{eff}}/2\mu$ is defined as the capillary diffusivity (units of m^2/s). In the particular case of pores with large aspect ratios, such as the alumina membranes obtained by electrochemical etching, r_{eff} coincides reasonably well to the pore size measured by electronic microscopy [39, 40]. Mesoporous silicon, also obtained through electrochemical etching, exhibit a sponge-like structure where the pores are interconnected, but maintaining a preferential direction perpendicular to its surface (z-axis) [41, 42]. The DBR here used is formed by alternating layers of porous silicon with different porosity, resulting in layers with different pore radius, as illustrated by the microscopy image in Figure 1c. In order to describe the fluid imbibition into a mesoporous matrix with such periodic structure, one may still consider an assembly of straight nanopores [19, 20, 42], now with periodic step changes in its radius, between r_{min} and r_{max}, along the axial z-direction, as schematized in Figure 1b. Actually, when capillary-driven flows advance through periodically constricted tubes, the LW dynamics holds but the effective radius in Eq. 4 now scales as $r_{\mathrm{eff}} \sim r_{\mathrm{min}}^4/r_{\mathrm{max}}^3$ [43, 44]. It is worth noting that this scaling ratio has been also observed in porous media with bimodal pore size distributions in the microscale [45, 46]. Thus, we consider Eq. 4 as a fair approximation for the purposes of this work.

As mentioned above, a key aspect is that the capillary diffusivity of the thermoplastic polymer employed as working fluid must present a temperature-dependent variation

coincident with the Arrhenius law. This feature can be found in thermoplastic polymers [47], where polymer viscosity is the controlling parameter. A typical example is pEVA, for a wide range of temperatures, as we demonstrated in a previous work [20]. Thus, one may write

$$D_c(T) = D_{c0} \exp\left(-\frac{E_{TTI}}{RT}\right), \tag{5}$$

where D_{c0} is a pre-exponential constant and E_{TTI} is the activation energy of molecular processes for fluid displacement, here considered as the activation energy of the TTI sensing system. In fact, inserting Eq. 5 in Eq. 4 and integrating yields

$$z^2 = D_{c0} \int_0^t \exp\left(-\frac{E_{TTI}}{RT}\right) \mathrm{d}t. \tag{6}$$

Taking into account that T is always a function of time, the filling degree of the structure, and hence the reflected color, depends on the undergone time-temperature history, which represents the deterioration level of the monitored product, that is,

$$z^2 = D_c(T_{ref})I. \tag{7}$$

Therefore, provided $E_{TTI} = E_{QI}$, the remaining shelf-life defined in Eq. 3 can be rewritten as follows

$$RSL = SL - \frac{z^2}{D_c(T_{ref})}. \tag{8}$$

Next step requires the coupling of Eq. 7 to the reflectance variation of the photonic crystal.

2.3. Optical response of the photonic crystal

The porous structure has a sequence of layers (Figure 1) with periodic step changes of porosity (p_i), resulting in a periodic variation of the refractive index (n_i). For this structure, the Bragg condition (preferential reflection of the reference wavelength λ_0) is reached when the optical path length, OPL (refractive index times thickness), of each layer satisfies $OPL_i = \lambda_0/4$. The presence of a polymer inside the pores increases the effective refractive index of each i-layer (Δn_i), and the variation of the OPL can be estimated as $\Delta\, OPL_i = \Delta n_i p_i z(t)$ [20]. Finally, taking into account Eq. 7 and provided $E_{TTI} = E_{QI}$, one has $\Delta\, OPL^2$ proportional to I, meaning that there is a specific reflected color for each value of the time-temperature history, thus encoding the sensor status.

3. Experimental

3.1. Materials

Crystalline p-type silicon (Topsil Semiconductor Materials SA, USA), doped with boron, orientation [100], and resistivity 1-5 mΩ·cm, was used to fabricate the DBRs. Fluorhydric acid (50%) and ethanol were used as received to prepare the electrolyte solution of the anodization process. Deionized water was used throughout the work. The polymer used to infiltrate the DBRs was pEVA (Elvax 260 from Dupont), which was thoroughly characterized in a previous work [20]. Here we reproduce some relevant physical properties: the polymer density at 23°C is 955 kg/m^3; the melting point is about 75°C; the weight-average molecular weight is 118000 g/mol; the radius of gyration is 22.1 nm; the polymer crystalinity is around 4.5%, and the refractive index is $n = 1.49$.

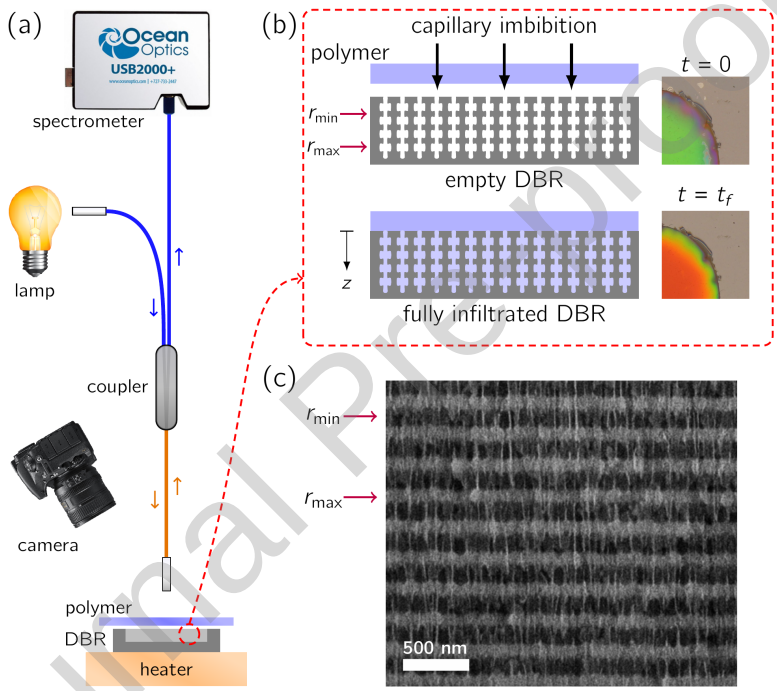

Figure 1: (a) Scheme of the experimental setup for measuring the DBR reflectance during polymer imbibition. (b) Highly schematic representation of polymer infiltration in the DBR, which is regarded an array of periodically constricted pores, with effective pore radius varying between $r_{\min}$ and $r_{\max}$ along the z-axis. The empty DBR reflects a well-defined wavelength (green), which is red-shifted when it is fully infiltrated with the polymer. (c) SEM image of the DBR showing the nanoscale periodic structurethat is formed by alternating layers of porous silicon with different porosity, which results equivalent to stratified layers with different pore radius ($r_{\min}$ and $r_{\max}$).

3.2. DBRs fabrication

The DBRs were prepared by electrochemical anodization of crystalline silicon, which serves as the anode of an electrochemical cell. The electrolyte consists in a solution of fluorhydric acid (50%) and ethanol (1:2) (v/v). The current density during anodization defines the mean pore size and porosity of the porous silicon formed. A profile of two current densities was applied to obtain a porous multilayer of two alternating porosities (DBR). The employed current densities were 59 mA/cm^2 and 106 mA/cm^2, which yielded porosities of 78 % and 86 %, respectively.The refractive index of each layer can be calculated by using the effective medium theory with an appropriate mixing rule. With the formulation proposed by Looyenga-Landau-Lifshitz [48], we obtained $n = 1.57$ and $n = 1.35$ for each layer. The DBR was designed for a reference wavelength $\lambda_0 = 530$ nm.

3.3. Optical measurements

The DBR reflectance variation during polymer imbibition was measured by using an UV-Vis-NIR spectrometer (Ocean Optics HR4000) provided with a R400-7-SR fiber-optic reflection probe. The DBR was placed onto a temperature-controlled plate with a temperature resolution of 0.1K. A thin layer of polymer was deposited onto the DBR surface. Subsequently, reflectance spectra were acquired at regular time intervals of 2s. A sequence of snapshots was captured from above by using a high-resolution digital camera (Canon EOS Rebel T5, Canon Inc., Tokyo, Japan) connected to a PC. The camera was positioned vertically 20 cm over the sample and manually focused. Images with a spatial resolution of about 20 µm per pixel were captured at intervals of 5 seconds. A scheme of the experimental setup is shown in Figure 1. In order to obtain the device response at different temperatures ($D_c(T)$) in a single experiment, the polymer imbibition process was performed by imposing a linear increase of temperature, as demonstrated in a previous work [20]. The position of the filling front and its time derivative were measured as a function of the time, and then used to obtain $D_c = 2z\frac{\mathrm{d}z}{\mathrm{d}t}$ (Eq. 4) as a function o time.

4. Results and discussion

Figure 2 shows the capillary diffusivity of the sensor as a function of temperature. The infiltrating polymer was pEVA and the DBR was formed by 50 layers of alternating pores sizes ($r_{\min}$ and $r_{\max}$), with 4.5 μm of total thickness. The layer of higher porosity ($r_{\max}$) was fabricated with an anodization current density of 106 mA/cm^2, while the current density corresponding to the lowest porosity layer ($r_{\min}$) was varied between 12 and 59 mA/cm^2. The linear behavior observed in the semilog plot is typical of Arrhenius-like processes. The curves are parallel since all of them correspond to the same polymer, which determines their slope: E_{TTI}/R, according to Eq. 5. Thus, the activation energy of the sensor can be found from Figure 2, which results in $E_{TTI} \approx 76$ kJ/mol. It is noted that increasing the temperature in about 40 °C increases D_c in more than three orders of magnitude, due to the thermally activated (Arrhenius-like) behavior of viscosity.

As mentioned above, the polymer has to be chosen on the base of temperature dependence of a specified QI, so that $E_{TTI} = E_{QI}$ in the temperature range of interest. For example, the E_{QI} for the general appearance of leafy greens is 65-70 kJ/mol [49], and for

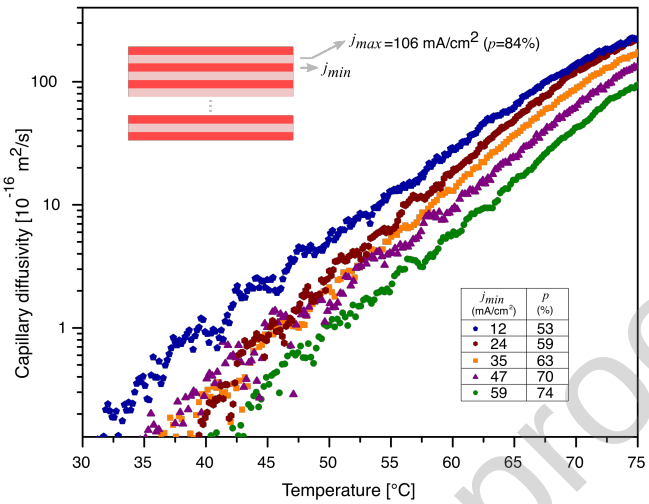

Figure 2: Capillary diffusivity for the imbibition of pEVA into the DBR formed by alternating layers with different porosity, which were fabricated by varying the current density (both parameters are reported in the inset). The stratified system thus combines layers with radii $r_{\max}$ and $r_{\min}$ that correspond to current densities $j_{\max}$ and $j_{\min}$, respectively ($j_{\max}$ was fixed, while $j_{\min}$ was varied; data in the inset).

the color of beef muscle is 81 kJ/mol [50]. Further, for a wide range of pharmaceuticals products, E_{QI} falls in the range 42-125 kJ/mol [51].

On the other hand, the relative position of the plots in the ordinate-axis of Figure 2 is set by the DBR pore structure, i.e. by the combination of $r_{\max}$ and $r_{\min}$, which allows tuning the reference level of the diffusivity (D_{c0} in Eq. 5). This result shows that $D_c(T)$ can be set by choosing a proper combination of thermoplastic polymer, with a particular $\mu(T)$, and the DBR structure ($r_{\max}$ and $r_{\min}$) for a given sensor application.

Figure 3a shows the reflectance spectra of the sensor for three different times (temperatures) during the polymer infiltration in a linear heating ramp experiment (current densities were 59 mA/cm^2 and 106 mA/cm^2). At $t = 0$, when the pores are still empty, the reflectance shows a peak at 530 nm and the sensor looks green. As time increases, the polymer infiltrates the pores and changes the Bragg condition of the sensor, consequently λ_0 shifts to a longer wavelength. As observed in Figure 3a, λ_0 moved to 680 nm after full infiltration of the DBR, which results in a red perception of the TTI. This shift is consistent with that expected when the air into the pores ($n = 1$) is replaced by the polymer ($n = 1.49$), as it can be calculated using the matrix formalism [52]. Variations of the DBR temperature could also affect the reflectance peak position due to the thermal expansion of the structure or by refractive index dependency with temperature. However, these variations are very small when compared to the changes produced by the imbibition of the polymer. Actually, we calculated that a temperature change of 40 ^{o}C would produces a resonance peak shift of less than 0.1 nm. Besides, concerning the temporal stability of the porous matrix, preliminary tests indicate that the reflectance peak position of empty DBR varies less than 3% after 30 days at ambient conditions, in accordance with previous reports [53].

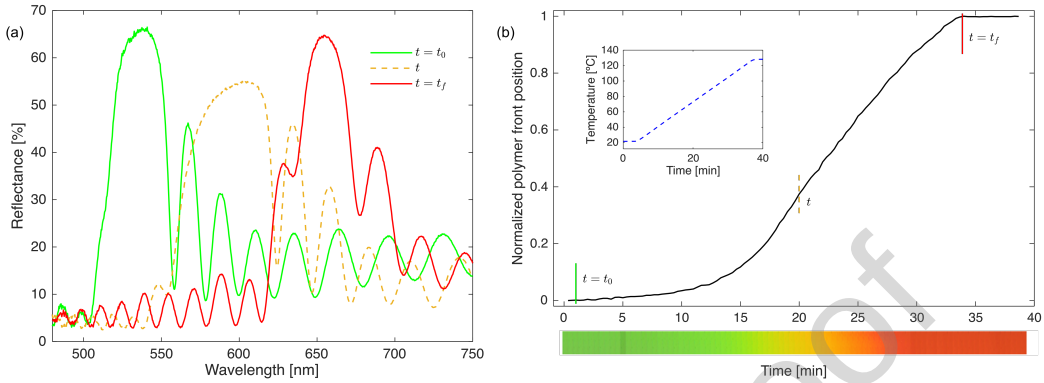

Figure 3: (a) Reflectance spectra obtained during polymer infiltration at $t = 0$ (empty pores), $t < t_f$ (partially-filled pores), and $t = t_f$ (fully-filled pores). (b) Reference wavelength position of the resonance peak as a function of time during polymer infiltration. The characteristic times corresponding to the spectra presented in (a) are also indicated. The inset shows the temperature ramp used in the experiment. The bottom color bar was constructed from individual snapshots of the sensor at each infiltration time.

Figure 3b shows the normalized polymer front position as a function of time during infiltration, for the temperature ramp shown in the inset. This position was obtained from the relative displacement of the reflectance peak in a spectrum zone that is not affected by high reflectance of the DBR [20]. All the experiments were carried out at least in duplicate; the run-to-run dispersion of the measured polymer front position was less than 2% (note that each experimental run involves a new device, since polymer imbibition into the matrix is irreversible). The color-bar shows the colors reflected by the sensor at each time, which are easily differentiated by the naked eye. This color-bar was constructed from a series of single snapshots of the sensor taken every 5 seconds during the temperature ramp.

Figure 4 shows the color-appearance of the sensor at different combinations of total exposure time and temperature. It was constructed from the snapshots of the sensor taken during polymer infiltration. As mentioned before, each value of filling position (z) is encoded with a particular color of the device (horizontal color-bar in Fig. 3b). Thus the 2D plot in Fig. 4 involves the calculation of z for each combination of time and temperature, using $z = \sqrt{D_c(T)t}$. Then, the color at each point shows the appearance of the sensor at each combination of total exposure time and temperature (green for the empty DBR and red for the fully infiltrated DBR). In other words, the color scale is a measure of the filling front position z, whereas each z value determines the corresponding time and temperature of occurrence (plotted as horizontal and vertical axis, respectively). For example, at 50°C , the TTI changes from green to red in about 1 day; however, the same color change takes about 10 days at 35°C. The slope and relative position of the color change zone (Arrhenius law, note the log-scale for the time-axis) can be adjusted from the polymer characteristics and the DBR structure. Thus one may tune the TTIs for the accurate monitoring of arbitrary QIs of food and pharmaceutical products.

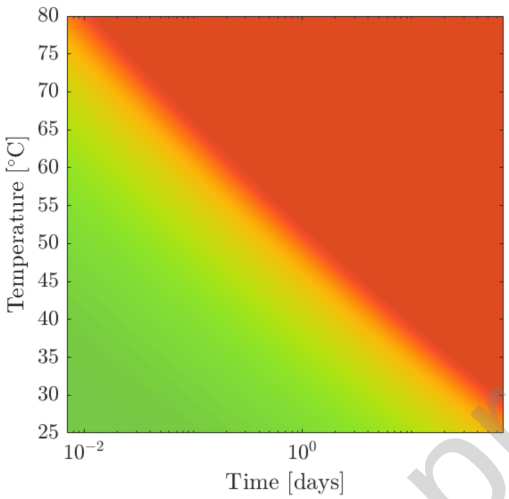

Figure 4: Time-temperature diagram built from the superposition of sensor snapshots: the color map represents the readout of the TTI after a cumulative temperature history.

5. Conclusions

In this work we demonstrate that the combination of (i) the sensing capacity of photonic crystals, (ii) the Arrhenius-like dependence of viscosity of thermoplastic polymers, and (iii) the spontaneous imbibition of a thermoplastic polymer into mesoporous silicon, together with the good repeatability of the process, can be exploited to build a reliable and completely autonomous TTI. The proposed device satisfies all the requirement to be used as a real-world TTI, namely: it is a flexible thin sheet, easy to pack, with irreversible response, naked-eye reading, and fine-tunability for different QIs. All these attributes make this sensor a good candidate to be employed for sensing the thermal history of perishable products, like food and pharmaceutical goods.

Acknowledgements

The authors thank the financial support received from Universidad Nacional del Litoral, CAI+D 50620190100114LI, Argentina.

References

[1] J. D. Selman, Time—temperature indicators, in: Active Food Packaging, Springer US, 1995, pp. 215–237. doi:10.1007/978-1-4615-2175-4_10.
URL https://doi.org/10.1007/978-1-4615-2175-4_10

[2] S. Wang, X. Liu, M. Yang, Y. Zhang, K. Xiang, R. Tang, Review of time temperature indicators as quality monitors in food packaging, Packaging Technology and Science 28 (10) (2015) 839–867. doi:10.1002/pts.2148.
URL https://doi.org/10.1002/pts.2148

[3] T. Gao, Y. Tian, Z. Zhu, D.-W. Sun, Modelling, responses and applications of time-temperature indicators (TTIs) in monitoring fresh food quality, Trends in Food Science & Technology 99 (2020) 311–322. doi:10.1016/j.tifs.2020.02.019.
URL https://doi.org/10.1016/j.tifs.2020.02.019

[4] L. Wang, Z. Wu, C. Cao, Technologies and fabrication of intelligent packaging for perishable products, Applied Sciences 9 (22) (2019) 4858. doi:10.3390/app9224858.
URL https://doi.org/10.3390/app9224858

[5] E. Drago, R. Campardelli, M. Pettinato, P. Perego, Innovations in smart packaging concepts for food: An extensive review, Foods 9 (11) (2020) 1628. doi:10.3390/foods9111628.
URL https://doi.org/10.3390/foods9111628

[6] H. Cheng, H. Xu, D. J. McClements, L. Chen, A. Jiao, Y. Tian, M. Miao, Z. Jin, Recent advances in intelligent food packaging materials: Principles, preparation and applications, Food Chemistry 375 (2022) 131738. doi:10.1016/j.foodchem.2021.131738.
URL https://doi.org/10.1016/j.foodchem.2021.131738

[7] M. Gou, G. Guo, J. Zhang, K. Men, J. Song, F. Luo, X. Zhao, Z. Qian, Y. Wei, Time–temperature chromatic sensor based on polydiacetylene (PDA) vesicle and amphiphilic copolymer, Sensors and Actuators B: Chemical 150 (1) (2010) 406–411. doi:10.1016/j.snb.2010.06.041.
URL https://doi.org/10.1016/j.snb.2010.06.041

[8] A. P. D. R. Brizio, C. Prentice, Use of smart photochromic indicator for dynamic monitoring of the shelf life of chilled chicken based products, Meat Science 96 (3) (2014) 1219–1226. doi:10.1016/j.meatsci.2013.11.006.
URL https://doi.org/10.1016/j.meatsci.2013.11.006

[9] B. Ye, J. Chen, H. Ye, Y. Zhang, Q. Yang, H. Yu, L. Fu, Y. Wang, Development of a time–temperature indicator based on maillard reaction for visually monitoring the freshness of mackerel, Food Chemistry 373 (2022) 131448. doi:10.1016/j.foodchem.2021.131448.
URL https://doi.org/10.1016/j.foodchem.2021.131448

[10] H. Vaikousi, C. G. Biliaderis, K. P. Koutsoumanis, Development of a microbial time/temperature indicator prototype for monitoring the microbiological quality of chilled foods, Applied and Environmental Microbiology 74 (10) (2008) 3242–3250. doi:10.1128/aem.02717-07.
URL https://doi.org/10.1128/aem.02717-07

[11] (Mar. 2019). doi:10.1016/j.ifset.2018.11.003, [link].
URL https://doi.org/10.1016/j.ifset.2018.11.003

[12] K. Kim, E. Kim, S. J. Lee, New enzymatic time–temperature integrator (TTI) that uses laccase, Journal of Food Engineering 113 (1) (2012) 118–123. doi:10.1016/j.jfoodeng.2012.05.009.
URL https://doi.org/10.1016/j.jfoodeng.2012.05.009

[13] P. Anbukarasu, D. Sauvageau, A. L. Elias, Time-temperature indicator based on enzymatic degradation of dye-loaded polyhydroxybutyrate, Biotechnology Journal 12 (9) (2017) 1700050. doi:10.1002/biot.201700050.
URL https://doi.org/10.1002/biot.201700050

[14] A. T. Pandian, S. Chaturvedi, S. Chakraborty, Applications of enzymatic time–temperature indicator (TTI) devices in quality monitoring and shelf-life estimation of food products during storage, Journal of Food Measurement and Characterization 15 (2) (2020) 1523–1540. doi:10.1007/s11694-020-00730-8.
URL https://doi.org/10.1007/s11694-020-00730-8

[15] C. Zhang, A.-X. Yin, R. Jiang, J. Rong, L. Dong, T. Zhao, L.-D. Sun, J. Wang, X. Chen, C.-H. Yan, Time–temperature indicator for perishable products based on kinetically programmable ag overgrowth on au nanorods, ACS Nano 7 (5) (2013) 4561–4568. doi:10.1021/nn401266u.
URL https://doi.org/10.1021/nn401266u

[16] A. T. Jafry, H. Lim, W.-K. Sung, J. Lee, Flexible time–temperature indicator: a versatile platform for laminated paper-based analytical devices, Microfluidics and Nanofluidics 21 (3) (Mar. 2017). doi:10.1007/s10404-017-1883-x.
URL https://doi.org/10.1007/s10404-017-1883-x

[17] L. T. Hao, M. Lee, H. Jeon, J. M. Koo, S. Y. Hwang, D. X. Oh, J. Park, Tamper-proof time–temperature indicator for inspecting ultracold supply chain, ACS Omega 6 (12) (2021) 8598–8604. doi:10.1021/acsomega.1c00404.
URL https://doi.org/10.1021/acsomega.1c00404

[18] R. Urteaga, C. L. A. Berli, Nanoporous anodic alumina for optofluidic applications, in: Nanoporous Alumina, Springer International Publishing, 2015, pp. 249–269. doi:10.1007/978-3-319-20334-8_8.

URL https://doi.org/10.1007/978-3-319-20334-8_8

[19] L. G. Cencha, G. Dittrich, P. Huber, C. L. Berli, R. Urteaga, Precursor film spreading during liquid imbibition in nanoporous photonic crystals, Physical Review Letters 125 (23) (Dec. 2020). doi:10.1103/physrevlett.125.234502.
URL https://doi.org/10.1103/physrevlett.125.234502

[20] L. G. Cencha, R. Urteaga, C. L. A. Berli, Interferometric technique to determine the dynamics of polymeric fluids under strong confinement, Macromolecules 51 (21) (2018) 8721–8728. doi:10.1021/acs.macromol.8b01504.
URL https://doi.org/10.1021/acs.macromol.8b01504

[21] H. Santos, Porous Silicon for Biomedical Applications, Woodhead Publishing Series in Biomaterials, Elsevier Science, 2021.
URL https://books.google.com.ar/books?id=R18lEAAAQBAJ

[22] U. S. Food, D. A. C. for Drug Evaluation, Research., Title 21, volume 3. part 177, subpart b, sec. 177.1350 ethylene-vinyl acetate copolymers.
URL https://www.accessdata.fda.gov/scripts/cdrh/cfdocs/cfcfr/cfrsearch.cfm?fr=177.1350

[23] M. Rack, Y. Belaroussi, K. B. Ali, G. Scheen, B. K. Esfeh, J.-P. Raskin, Small- and large-signal performance up to 175 °c of low-cost porous silicon substrate for RF applications, IEEE Transactions on Electron Devices 65 (5) (2018) 1887–1895. doi:10.1109/ted.2018.2818466.
URL https://doi.org/10.1109/ted.2018.2818466

[24] R. P. Arens, R. D. Birkholz, D. L. Johnson, T. P. Labuza, C. L. Larson, D. J. Yarusso, Time-temperature integrating indicator device (Sep. 1997).

[25] M. A. Jozefowicz, Liquid and/or temperature activated elapsed time indicators suitable, in particular, as doneness indicators for foodstuffs (Jan. 1993).

[26] H. Norrby, M. Nygardh, Label having a temperature-monitoring function, a package for goods provided with a label, as well as a method and equipment for the application of labels to packages for goods (Feb. 2011).

[27] W. J. Manske, Selected time interval indicating device (May 1976).

[28] F. Zhang, X. Xu, J. He, B. Du, Y. Wang, Highly sensitive temperature sensor based on a polymer-infiltrated mach–zehnder interferometer created in graded index fiber, Optics Letters 44 (10) (2019) 2466. doi:10.1364/ol.44.002466.
URL https://doi.org/10.1364/ol.44.002466

[29] B. Du, J. He, M. Yang, Y. Wang, X. Xu, J. Wang, Z. Zhang, F. Zhang, K. Guo, Y. Wang, Highly sensitive hydrogen sensor based on an in-fiber mach-zehnder interferometer with polymer infiltration and pt-loaded WO3 coating, Optics Express 29 (3) (2021) 4147. doi:10.1364/oe.417424.
URL https://doi.org/10.1364/oe.417424

[30] A. Leal-Junior, A. Frizera-Neto, C. Marques, M. Pontes, A polymer optical fiber temperature sensor based on material features, Sensors 18 (2) (2018) 301. doi:10.3390/s18010301.
URL https://doi.org/10.3390/s18010301

[31] A. G. Leal-Junior, C. A. Díaz, A. Frizera, C. Marques, M. R. Ribeiro, M. J. Pontes, Simultaneous measurement of pressure and temperature with a single FBG embedded in a polymer diaphragm, Optics & Laser Technology 112 (2019) 77–84. doi:10.1016/j.optlastec.2018.11.013.
URL https://doi.org/10.1016/j.optlastec.2018.11.013

[32] A. Arsenault, Temperature-responsive photonic crystal device (Feb. 2012).

[33] P. S. Chan, K. M. Yeung, M. Chang, S. M. Lee, Time temperature indicator by chromatography and photonic lattices change (Jan. 2017).

[34] M. A. van Boekel, Kinetic modeling of food quality: A critical review, Comprehensive Reviews in Food Science and Food Safety 7 (1) (2008) 144–158. doi:10.1111/j.1541-4337.2007.00036.x.
URL https://doi.org/10.1111/j.1541-4337.2007.00036.x

[35] P. TAOUKIS, T. LABUZA, Reliability of time-temperature indicators as food quality monitors under nonisothermal conditions, Journal of Food Science 54 (4) (1989) 789–792. doi:10.1111/j.1365-2621.1989.tb07883.x.
URL https://doi.org/10.1111/j.1365-2621.1989.tb07883.x

[36] T. Labuza, L. Szybist, Open Dating of Foods, Publications in food science and nutrition, Wiley, 2008.
URL https://books.google.com.ar/books?id=63gD4zUfLeIC

[37] R. Lucas, Ueber das zeitgesetz des kapillaren aufstiegs von flüssigkeiten, Kolloid-Zeitschrift 23 (1) (1918) 15–22. doi:10.1007/bf01461107.
URL https://doi.org/10.1007/bf01461107

[38] E. W. Washburn, The dynamics of capillary flow, Phys. Rev. 17 (1921) 273–283. doi:10.1103/PhysRev.17.273.
URL https://link.aps.org/doi/10.1103/PhysRev.17.273
[39] R. Urteaga, L. N. Acquaroli, R. R. Koropecki, A. Santos, M. Alba, J. Pallarès, L. F. Marsal, C. L. A. Berli, Optofluidic characterization of nanoporous membranes, Langmuir 29 (8) (2013) 2784–2789. doi:10.1021/la304869y.
URL https://doi.org/10.1021/la304869y
[40] L. G. Cencha, P. Huber, M. Kappl, G. Floudas, M. Steinhart, C. L. A. Berli, R. Urteaga, Non-destructive high-throughput screening of nanopore geometry in porous membranes by imbibition, Applied Physics Letters 115 (11) (2019) 113701. doi:10.1063/1.5119338.
URL https://doi.org/10.1063/1.5119338
[41] L. Canham, Handbook of Porous Silicon, Springer International Publishing, 2018.
URL https://books.google.com.ar/books?id=eo3UwAEACAAJ
[42] L. N. Acquaroli, R. Urteaga, C. L. A. Berli, R. R. Koropecki, Capillary filling in nanostructured porous silicon, Langmuir 27 (5) (2011) 2067–2072. doi:10.1021/la104502u.
URL https://doi.org/10.1021/la104502u
[43] C. L. A. Berli, M. Mercuri, M. G. Bellino, Modeling the abnormally slow infiltration rate in mesoporous films, Physical Chemistry Chemical Physics 19 (3) (2017) 1731–1734. doi:10.1039/c6cp06602j.
URL https://doi.org/10.1039/c6cp06602j
[44] M. Sallese, J. Torga, E. Morel, N. Budini, R. Urteaga, Optical coherence tomography measurement of capillary filling in porous silicon, Journal of Applied Physics 128 (2) (2020) 024701. doi:10.1063/1.5145270.
URL https://doi.org/10.1063/1.5145270
[45] F. Dullien, M. El-Sayed, V. Batra, Rate of capillary rise in porous media with nonuniform pores, Journal of Colloid and Interface Science 60 (3) (1977) 497–506. doi:10.1016/0021-9797(77)90314-9.
URL https://doi.org/10.1016/0021-9797(77)90314-9
[46] D. Patro, S. Bhattacharyya, V. Jayaram, Flow kinetics in porous ceramics: Understanding with non-uniform capillary models, Journal of the American Ceramic Society 90 (10) (2007) 3040–3046. doi:10.1111/j.1551-2916.2007.01776.x.
URL https://doi.org/10.1111/j.1551-2916.2007.01776.x
[47] C. Macosko, Rheology: Principles, Measurements, and Applications, Wiley, 1994.
URL https://books.google.com.ar/books?id=Kai7QgAACAAJ
[48] L. D. Landau, E. M. Lifshitz, L. P. Pitaevskii, Electrodynamics of continuous media, 2nd Edition, Butterworth-Heinemann, Oxford, England, 1984.
[49] A. Mishra, R. L. Buchanan, D. W. Schaffner, A. K. Pradhan, Cost, quality, and safety: A nonlinear programming approach to optimize the temperature during supply chain of leafy greens, LWT 73 (2016) 412–418. doi:10.1016/j.lwt.2016.06.037.
URL https://doi.org/10.1016/j.lwt.2016.06.037
[50] B. Ling, J. Tang, F. Kong, E. J. Mitcham, S. Wang, Kinetics of food quality changes during thermal processing: a review, Food and Bioprocess Technology 8 (2) (2014) 343–358. doi:10.1007/s11947-014-1398-3.
URL https://doi.org/10.1007/s11947-014-1398-3
[51] H. P. R. A. (HPRA), Guide to control and monitoring of storage and transportation conditions, https://www.hpra.ie/homepage/about-us/publications-forms/guidance-documents/item?id=5060f925-9782-6eee-9b55-ff00008c97d0&t=/docs/default-source/publications-forms/guidance-documents/ia-g0011-guide-to-control-and-monitoring-of-storage-and-transportation-conditions-v3 (Oct 2020).
[52] E. Osorio, R. Urteaga, H. Juárez, R. Koropecki, Transmittance correlation of porous silicon multilayers used as a chemical sensor platform, Sensors and Actuators B: Chemical 213 (2015) 164–170. doi:10.1016/j.snb.2015.02.058.
URL https://doi.org/10.1016/j.snb.2015.02.058
[53] T. D. James, G. Parish, C. A. Musca, A. J. Keating, N[sub 2]-based thermal passivation of porous silicon to achieve long-term optical stability, Electrochemical and Solid-State Letters 13 (12) (2010) H428. doi:10.1149/1.3489075.
URL https://doi.org/10.1149/1.3489075

Biographies:

Luisa G. Cencha received her B.Sc. degree in materials science and Ph.D. degree from the Universidad Nacional del Litoral (Argentina) in 2014 and 2018, respectively. She is currently a Postdoctoral Researcher at INTEC (National Council for Scientific and Technological Investigations), Santa Fe, Argentina. Her research interests include microfluidics, photonic materials, and condensed matter under confinement.

Fernanda G. Garcia received her degree in Chemical Engineering from the Universidad Nacional del Litoral, Argentina, in 2021. During the last part of her career, she performed research practices at IFIS-Litoral, Santa Fe, Argentina.

Nicolas Budini received his BS and PhD degrees in physics in 2007 and 2012, respectively. He is an assistant professor in the Physics Department of the Faculty of Chemical Engineering at National University of Litoral, Santa Fe, Argentina. He is also a fellow researcher at the Group of Semiconductor Physics of the Litoral Institute of Physics, Santa Fe, Argentina. His current research interests include optical metrology techniques like digital holography, digital holographic interferometry, digital holographic microscopy, used in the fields of semiconductors and microfluidics.

Raúl Urteaga received the Laurea degree and the Ph.D. degree in physics from the Balseiro Institute, San Carlos de Bariloche, Argentina, in 2000 and 2008 respectively. Currently he is full professor at the Department of Physics, FIQ-UNL, and Researcher of the National Council for Scientific and Technological Investigations (CONICET), at IFIS-Litoral, Santa Fe, Argentina. His research interests include nanostructured porous semiconductors, interferometry and microfluidics.

Claudio L.A. Berli received a bachelor's degree in Biochemistry and PhD in Chemical Technology from National University of Litoral (UNL), Argentina. Then he held a postdoctoral position at the University of Paris, in the field of physicochemical hydrodynamics. Currently he is full professor at the Department of Basic Sciences, UNL, and Researcher of the National Council for Scientific and Technological Investigations (CONICET), at INTEC, Santa Fe, Argentina. His research interests include the fundamentals and applications of microfluidics and lab-on-a-chip devices.

Graphical abstract

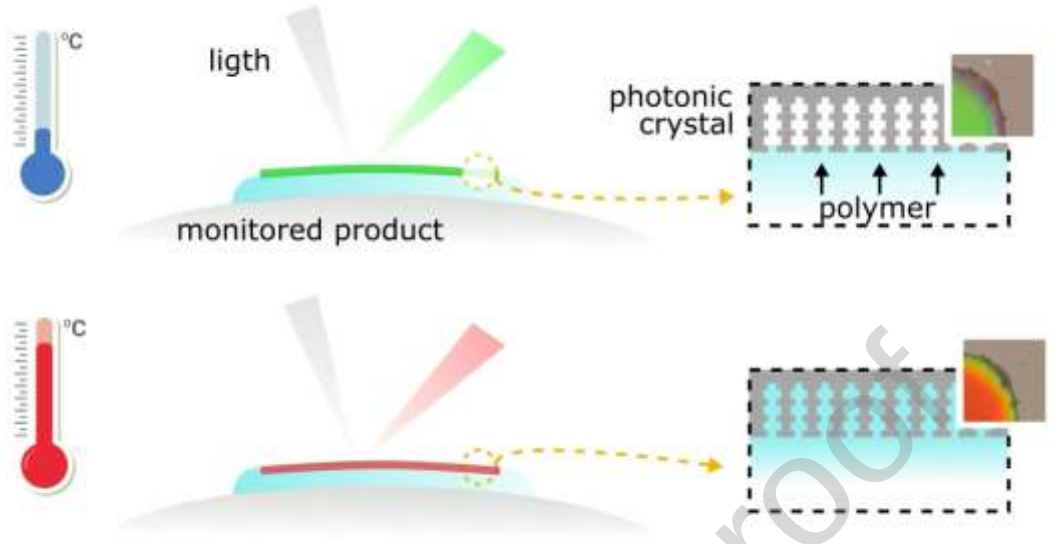

Luisa G. Cencha: Investigation, Formal analysis, Writing

Fernanda G. Garcia: Investigation

Nicolas Budini: Metodology, Formal analysis, Writing

Raúl Urteaga: Metodology, Software, Formal analysis, Writing, Funding acquisition

Claudio L. A. Berli: Conceptualization, Writing - Review & Editing, Project administration

Declaration of interests

☒The authors declare that they have no known competing financial interests or personal relationships that could have appeared to influence the work reported in this paper.

☐The authors declare the following financial interests/personal relationships which may be considered as potential competing interests:

- A time-temperature sensor with straightforward and intuitive readout was developed
- The sensor combines 1D porous silicon photonic crystals and thermoplastic polymers
- The optical response is tunable from polymer characteristics and photonic crystal structure
- The device is thin, flexible, easy to pack, and presents irreversible cumulative information